Journal of Engineering and Technology Research Vol. 3(7), pp. 209-216, July 2011
Available online at http://www.academicjournals.org/JETR
ISSN 2006-9790 ©2011 Academic Journals

Full Length Research Paper

Two-dimensional particle modeling of submicrometer ZnO MESFET based on an ensemble Monte Carlo calculation including five-valley band structure model

H. Arabshahi[1,2]

[1]Department of Physics, Ferdowsi University of Mashahd, Mashhad, Iran
[2]Department of Physics, Payame Nour University of Fariman, Fariman, Iran. E-mail: arabshahi@um.ac.ir.

Accepted 27 May, 2011

A Monte Carlo method has been developed for the study of electron transport properties in ZnO MESFET for high field, using a five-valley conduction band model. The effects of upper valleys on the characteristics of ZnO MESFETs have been investigated. The following scattering mechanisms, that is impurity, polar optical phonon, acoustic phonon, alloy and piezoelectric are included in the calculation. Ionized impurity scattering has been treated beyond the born approximation using the phase-shift analysis. The simulation results show that on the drain side of the gate region, hot electrons attained enough energy to be scattered into the upper satellite conduction valleys. Approximately 17% of the electrons occupy the higher valleys (mainly *U* and *M* valley). The simulated device geometries and doping are matched to the nominal parameters described for the experimental structures as closely as possible, and the predicted drain current and other electrical characteristics for the simulated device including upper valleys show much closer agreement with the available experimental data.

Key words: Particle modeling, submicrometer, ionized impurity, polar optical phonon.

INTRODUCTION

In recent years, devices made from ZnO have attracted considerable interest because of its potential for short-wavelength photonic devices and high-power, high-frequency electronic devices (Allen et al., 2010). Up to now mostly metal-insulator-semiconductor structures (MISFETs) are used for those purposes due to the simple realization of high-*k* insulators by *rf*-sputtering techniques (Grundmann et al., 2010). However, the key advantage of metal-semiconductor FETs (MESFETs) is the higher mobility of carriers in the channel, as compared to MISFETs. Since the carriers in the channel of a MISFET are accelerated toward the semiconductor/insulator interface by the gate electric field where they suffer interface scattering, their mobility is less than half of the mobility of bulk material (Nemec et al., 2010). As the depletion region in MESFETs keeps the carriers off the gate interface, their mobility is close to that of bulk material. The higher mobility leads to a higher current, transconductance and transit frequency of the device (Arabshahi et al., 2007). In this article, we present a two dimensional ensemble Monte Carlo simulation of electron transport in ZnO MESFET (Cameron et al., 1983). Our current approach employs a valley conduction band model to investigate steady-state electron transport in this device (Arabshahi, 2007). However, the momentum space treatment is three dimensional, and the scattering events consider all three dimensions. Specifically, our model includes the five lowest valleys of the conduction band with nonparabolicity (Cameron et al., 1982). The device geometries and transport model are described in “model, device and simulations”, after which the simulation results are thus provided. Subsequently, details of the device fabrication and simulation model which is used in the characteristic of the device are presented, after which details of the effects of upper valley in ZnO MESFET and the results obtained are interpreted.

MODEL, DEVICE AND SIMULATIONS

Our self-consistent MonteCarlo simulation was performed using an analytical band structure model consisting of five non-parabolic

ellipsoidal valleys. The pseudo potential band structure shows the conduction band minimum to be located at the Γ point (Γ_1), and lowest energy conduction band satellite valleys to occur at the *U*point (located about two thirds of the way between the *L* and *M* symmetry points). Higher conduction band valleys are located at the Γ point (Γ_3), at the M point, and at the *K* point (Figure 1). In our Monte Carlo simulation, the two different Γ valleys, the six equivalent *U* valleys, the three equivalent *M* valleys and the two equivalent *K* valleys are represented by ellipsoidal, non-parabolic dispersion relationships of the following form (Jacoboni et al., 1989).

$$E(k)[1+\alpha_i E(k)] = \frac{\hbar^2}{2}\left[\frac{k_x^2+k_y^2}{m_\perp^*}+\frac{k_z^2}{m_\parallel^*}\right] \quad (1)$$

where $m_\perp^*$ and $m_\parallel^*$ are the transverse and longitudinal effective masses at the band edge and α_i is the non-parabolicity coefficient of the *i*-th valley.

Material parameters such as nonparabolicities, valley separations, and transverse and longitudinal effective masses are obtained either from experimental results or from pseudopotential calculations (Table 1). A constant time step discretization scheme is chosen in the Monte Carlo procedure, which allows us to track the time evolution of the electronic transport as well as to determine the position of all sample electrons at given instances of time. Consequently, the electron concentration as a function of space and time can be determined and Poisson's equation can be solved to obtain the self-consistent electric field. The modeled structure is divided into three regions, as indicated. Electron particles are initially distributed keeping all regions charge neutral. The location of the source and the drain implants and the top and back buffer layer are marked (Arabshahi et al., 2007).

In order to minimize the statistical fluctuations, always associated with the stochastic Monte Carlo method, we choose 20000 electron particles for the simulation and a time step of 10 fs for the readjustment of the electric field. A charge assignment scheme is also used to suppress the fluctuations. Each particle represents a cloud of electrons. The charge of the particle is assigned to its nearest four background mesh points proportionally to the position of the particle in the cell. To make the charge assignment more efficient, field cell size used for the central region is 30 nm^2 (horizontal × vertical), but that in the high doped source and drain implants is finer (10 nm^2).

Electrons in the bulk are scattered by ionized impurities and by bulk acoustic and non-polar optical phonon modes. Intervalley scattering by the absorption and emission of long wavelength acoustic and optic phonons have also been considered in the model. As described in detail, model devices are built up as a series of joined rectangular regions, with the electric field cell sizes matched along the join between each region. Each region can consist of multiple layers of different alloy composition and doping/compensation density. The ZnO MESFET can be described simply by three regions (Figure 1), representing source and drain doping implants and a central region containing the supply layers.

Figure 1 shows a schematic of the modeled ZnO MESFET. The overall device length is 3.3 µm in the *x*-direction and the device has a 0.3 µm gate length and 0.5 µm source and drain length. The source and drain have Ohmic contacts and gate is in Schottky contact in 1 eV to represent the contact potential at Au/Pt. The source and drain regions are doped to 5×10^{23} m^{-3} electron concentration and the top and down buffer layers are doped to 2×10^{23} and 1×10^{22} m^{-3} electron concentration, respectively. The geometry of the device to be simulated is specified at the beginning of the simulation by defining it in an *x-y* plane as a set of joined rectangular regions, each with uniform doping and other material parameters, and a set of contact regions. All physical quantities are assumed constant in the *z* direction (device width).

RESULTS

Figure 2 compares the instantaneous distribution of electrons throughout the device in the steady-state for different gate and drain biases at room temperature. When a positive potential V_{ds} is applied to the drain, electrons flow from source to drain, giving a current I_{ds} from source to drain. The depletion region of the Schottky barrier restricts the current path to the lower part of the channel and the buffer layer. At zero drain bias (Figure 2a), the depletion layer beneath the gate has a symmetric shape. At zero gate and drain bias, the depletion region corresponds to that associated with the built-in potential of the Schottky barrier, but is larger for the case of gate bias V_{gs}=-1 V shown here. As V_{ds} is increased from zero, the depletion layer becomes asymmetric in shape since the potential difference between the gate and the channel is greater at the drain end than the source end of the gate. The channel is more constricted at the drain end of the gate and the field along the channel is also higher in that region.

As the drain-source voltage is increased further, the field at the drain end of the gate approaches the value at which the electron velocity along the channel saturates. Beyond this value, which corresponds to the threshold voltage in the drain current-voltage characteristics, further increase in drain-source voltage does not substantially increase the drain-source current. The length of the region of the channel over which the electrons are in velocity saturation increases and there is some carrier accumulation within the channel. The depletion layer edge at the drain end of the gate also moves closer to the drain as the drain-source voltage increases. Note also that the transition between the gate depletion region and the charge neutral bulk is far from sharp on the drain side. At a sufficiently negative gate potential the depletion layer punches through to the high-resistively buffer layer, and the source and drain electrodes are connected only by leakage paths within the buffer layer and substrate (Figure 2b).

An important factor in the high frequency performance of the MESFET is the time taken for electrons to traverse the region of the device beneath the gate, and the performance is enhanced by a high average electron velocity through that region. The spatial distribution of hot electrons throughout the device for each valley at V_{gs}=-1 V and V_{ds}=30 V for room temperature operation is shown in Figure 3. Electrons are seen to exist in the upper valleys only to the right of the high field region, which exists on the drain side of the gate, because it is only there that the electrons have attained enough energy to be scattered into the satellite conduction valleys. Also note there is an injection of electrons from the channel into the buffer layer; a process which is eventually

Table 1. Important parameters used in our simulations for ZnO material (Foutz et al., 1997).

Parameter	ZnO
Density (kgm^{-3}) (Allen et al., 2010)	3200
Sound velocity (ms^{-1}) (Arabshahi et al., 2007)	1373
Static relative permitivity ε_0	9.7
Optical relative permitivity ε_∞	6.5
Deformation potential (eV)	15
Polar optical phonon energy (meV)	120
Energy gap (eV) (Nemec et al., 2010)	3.43
Intervalley deformation potential (10^7 eVm^{-1})	0.356
Nonparabolocity (eV^{-1}), (Arabshahi et al., 2007)	3.39 0.323

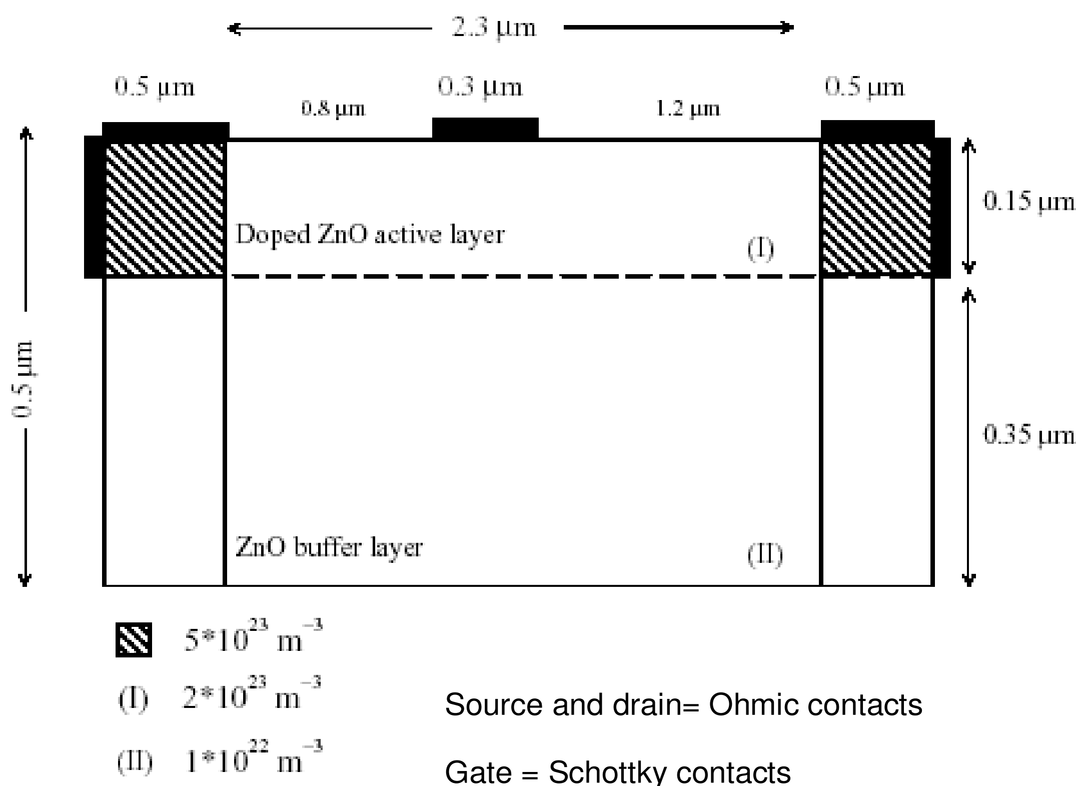

Figure 1. The two-dimensional model of ZnO MESFET.

opposed by the electric field created by the resulting negative space charge in the buffer layer. Figure 3 also shows that the distribution of electrons occupying the upper valleys extends a significant way towards the drain region where the electric field is much lower. This is a result of the finite time that it takes for phonon scattering to return the electrons to the Γ-valley.

Figure 4 shows the valley electron occupancies throughout the device. It can be seen that significant electron transfer to the upper valleys only begins to occur under the gate. Approximately 17% of the electrons occupy the higher valleys (mainly *U* and *M* valleys) in the vicinity of the gate which is similar to the valley occupancy ratio in the active layer of the n^+-n-n^+ diode. Figure 5 shows various microscopic properties of the device when the source-drain bias is 30 V and the gate voltage is -1 V; specifically the longitudinal electric field, the Γ-valley band profile, the electron kinetic energy, the

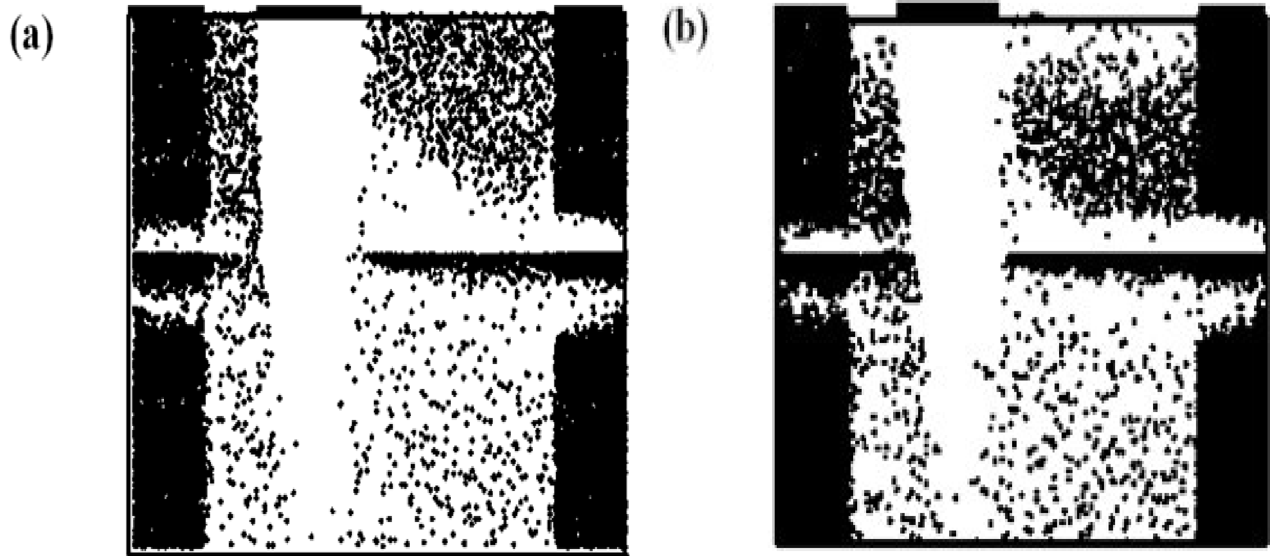

Figure 2. Depletion layer profiles for different drain and gate biases for ZnO MESFET at room temperature.

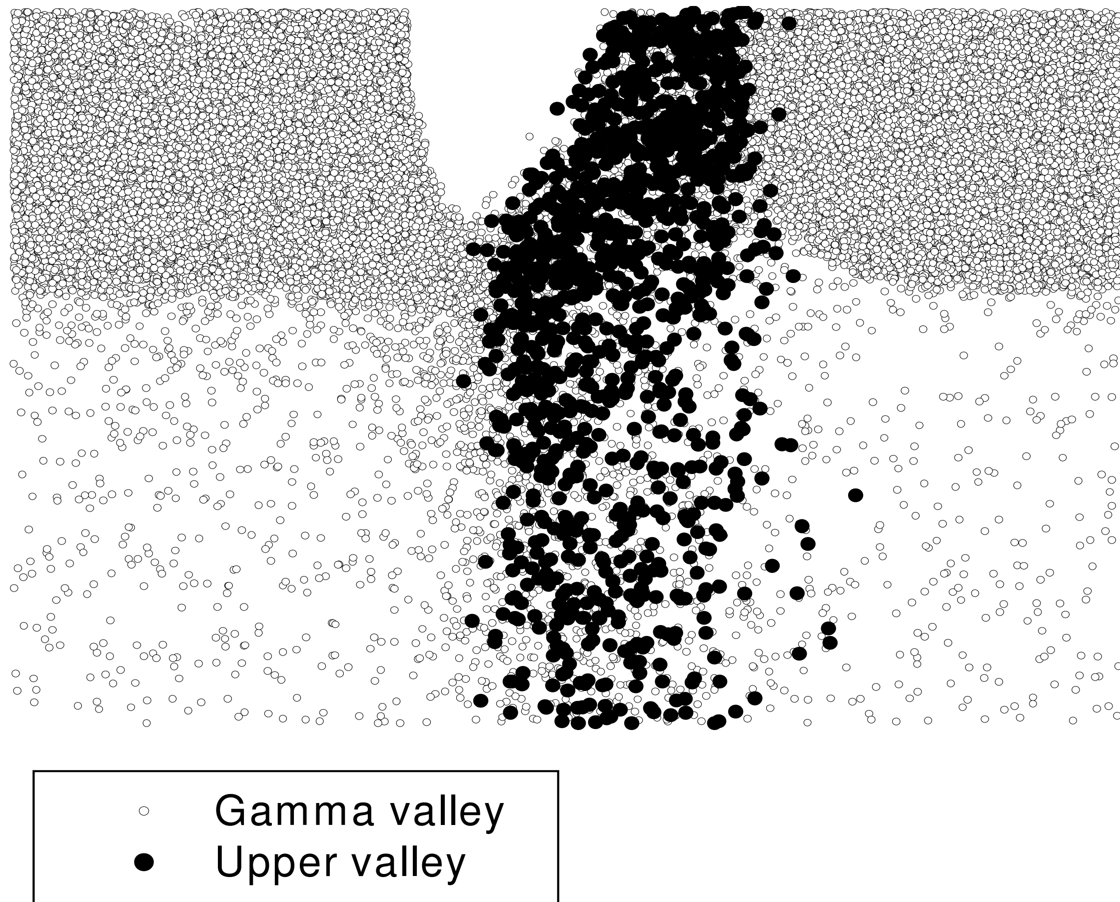

Figure 3. The distribution of hot electrons at room temperature for V_{gs}=-1 V_{ds}=30 V in central Γ valley and upper valleys.

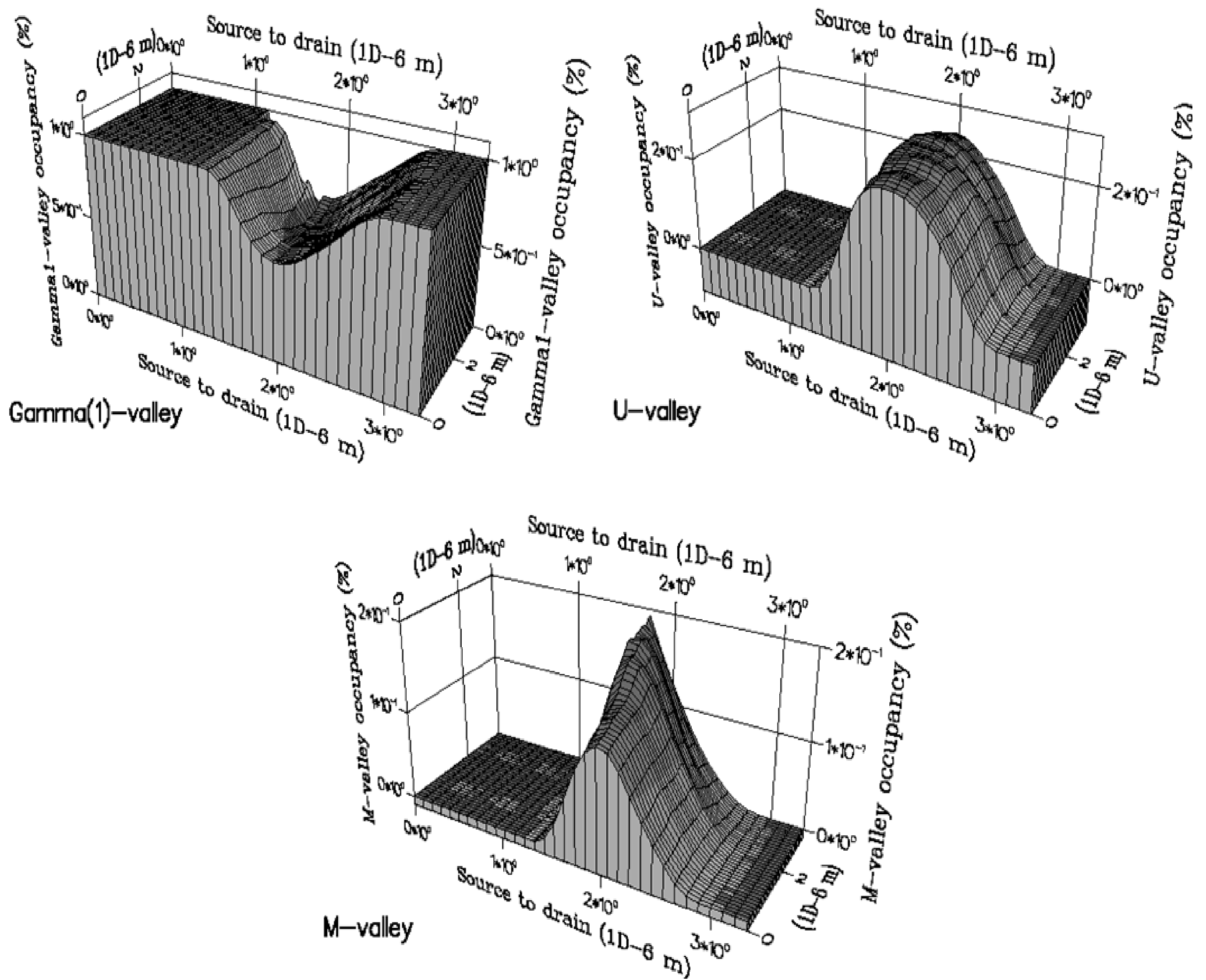

Figure 4. The valley occupation ratios for the central Γ_1-valley and upper valleys when the source-drain bias is 30 V and the gate voltage is -1 V at T=300 K.

average drift velocity and the total electron density as a function of distance from the source. The longitudinal electric field plotted in Figure 5a shows the high electric field in the region under the gate, which has been referred to earlier. Related to this is the Γ-valley band profile throughout the device in Figure 5b. Note almost all the drain-source potential is dropped within the gate-drain region, leaving a flat potential profile near the source and drain. As electrons move towards the drain, they lose potential energy and gain sufficient kinetic energy to transfer to the upper conduction valleys where their drift velocity is reduced.

The variations of average electron kinetic energy and average drift velocity throughout the simulated device are shown in Figures 5c and d, respectively. The average electron velocity reaches about 2×10^5 ms^{-1} and then declines towards the drain. The steep decrease in the average kinetic energy on the drain side of the gate is due to the transfer of electrons to the upper valleys. The electron density through the device is shown in Figure 5e. The gate depletion region is clearly seen where the electron density is several orders of magnitude lower than it is near the source and drain.

The drain current is obtained by counting the net charge flow through the drain contact. Figures 6a and b show the calculated drain current versus drain-source voltage at different gate biases for temperatures of 300 and 420 K. The simulated characteristics at 300 K show good saturation behavior with a knee voltage around 15 to 20 V and a saturation drain current of about 1200 mA/mm for V_{gs}=0 V. The high drain current density is encouraging for the use of ZnO for high-power applications.

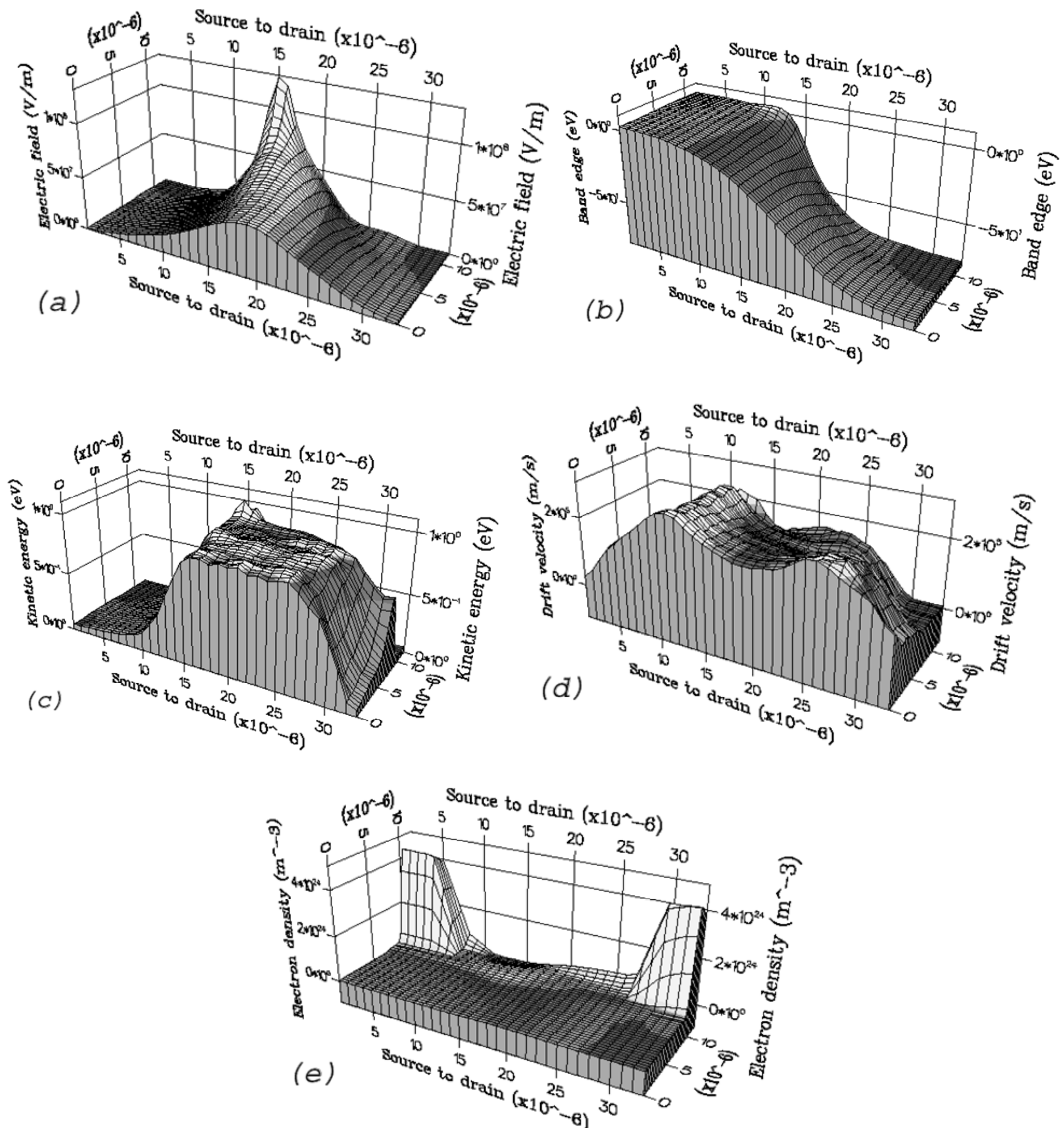

Figure 5. Three dimensional distribution of electron data recorded through the simulation of the GaN MESFET when the source-drain bias is 30 V and the gate voltage is -1 V at room temperature. This figure shows: (a) Longitudinal electric field, (b) Γ-valley conduction band profile, (c) Average kinetic energy, (d) Drift velocity and (e) Electron density. At V_{ds}= 80 V essentially the whole drain current flows entirely through the buffer.

From Figure 6a it is clear that the device is not completely pinched-off even at large negative gate bias (V_{gs}=-6 V) which is due to strong electron injection into the buffer layer at high electric fields. An increasing fraction of the drain current flows through the buffer as the drain voltage increases.

To obtain some idea of the effect of high temperature on ZnO MESFETs, simulations were carried out at T= 420 K, keeping the other device parameters unchanged. The *I-V* curves obtained are shown in Figure 6b.

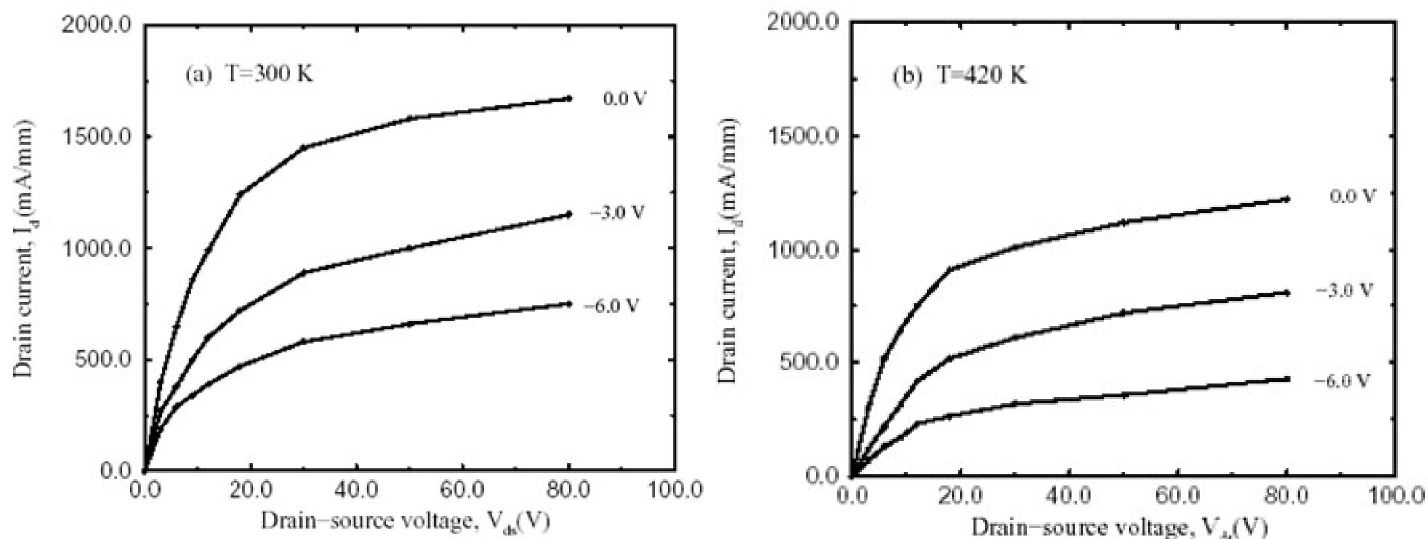

Figure 6. (a) The simulated drain current versus drain voltage at T= 300 K, (b) The simulated drain current versus drain voltage at T= 420 K.

Comparing the *I-V* curves at T= 300 and 420 K, it can be seen that the drain current is somewhat lower at the higher temperature, due to increased phonon scattering, but the effect is not major.

Figure 6 shows the general shape of the simulated *I-V* characteristics is similar to the experimental measurements but the predicted drain currents are higher. This discrepancy could be explained by electron trapping effects which are thought to play an important role in the electrical properties of ZnO devices due to the current limitations of the material technology. On applying drain bias, electrons passing from source to drain will have a certain probability of being captured. Emission of trapped electrons will also occur with a certain probability and in the steady-state there will be a density of trapped electrons determined by the balance between capture and emission. Hence, for any given electron there will be additional processes of electron capture and re-emission during electron transport and the effective transit time will be increased. In addition the trapped electrons cause space charge which acts to reduce the drain current. The transconductance of the MESFET is given by (Moglestue, 1993)

$$g_m = \frac{\Delta I_d}{\Delta V_g}\Big|_{V_d} \quad (2)$$

and is calculated from Figure 6a to be about 150 mS/mm at 18 V drain bias and -1 V gate voltage for room temperature. When the drain bias is increased to 30 V at the same gate voltage , the transconductance increases approximately to 220 mS/mm. In comparison, good GaAs MESFETs without a gate recess have a transconductance around 110 mS/mm. The higher value of transconductance in simulated ZnO MESFET is related to a higher drain current.

Conclusions

In summary, Monte Carlo simulations of electron transport in ZnO MESFET for temperatures greater than 300 K, using an approximate band structure comprised of five analytic conduction band valleys yield higher valleys are important, because more than 17% of the electrons occupy the higher valleys (mainly *U* and *M* valley) which will produce a serious reduction in the drain current and consequently the output power of ZnO MESFET. Our calculations indicate that the high temperature output drain current is limited by strong polar optical phonon scattering.

REFERENCES

Allen MW, Swartz CH, Myers TH, Veal TD, Durbin SM (2010). Bulk transport measurements in ZnO: The effect of surface electron layers. Phys. Rev., 81: 075211.

Arabshahi H, Benam MR, Salahi B (2007). A Shock-Capturing Upwind Disceritization Method For Characterization of SiC MESFETs. Mod. Phys. Lett. B., 21: 1715.

Arabshahi H (2007). Monte Carlo Modeling of Hot Electron Transport in Bulk AlAs, AlGaAs and GaAs at Room Temperature. Mod. Phys. Lett. B., 21: 199.

Cameron DC, Irving LD, Whitehouse CR (1983). Comparison of High and Low Field Electron Transport in AlGaN, AlN and GaN. Thin Solid

Films, pp. 103-161.

Cameron DC, Irving LD, Whitehouse CR (1982). Comparison of Low Field Electron Transport in ZnO and GaN Structures for High-Power and high Temperature Device Modelling, Electron. Lett., pp. 18-534.

Foutz BE, Eastman LF, Bhapkar UV, Shur M (1997). Discretization Method of Hydrodynamic for simulation of ZnO MESFETs. Appl. Phys. Lett., 70: 2849.

Grundmann M, Frenzel H, Lajn A, Lorenz M, Schein F, Wenckstern H (2010). Transparent semiconducting oxides: Materials and devices. Physica Status Solidi (a), 207: 1269.

Jacoboni C, Lugli P (1989). The Monte Carlo Method for semiconductor and Device Simulation. Springer-Verlag.

Moglestue C (1993). Monte Carlo Simulation of Semiconductor Devices. Chapman and Hall.

Nemec H, Rochford, J, Taratula O, Sundstrom (2010). Influence of the Electron-Cation Interaction on Electron Mobility in Dye-Sensitized ZnO and TiO_2 Nanocrystals: A Study Using Ultrafast Terahertz Spectroscopy. Phys. Rev. Lett., 104: 197401.